

Structure and morphology effects on sensing properties $\text{Cd}_x\text{Pb}_{1-x}\text{S}$ films

© L.N. Maskaeva^{1,2}, I.V. Vaganova^{1,2}, V.F. Markov^{1,2}, A.E. Bezdetnova^{1,2}, A.D. Selyanina^{1,2},
V.I. Voronin³, I.O. Selyanin^{1,4}

¹ Ural Federal University after the first President of Russia B.N. Yeltsin,
620002 Yekaterinburg, Russia

² Ural Institute of State Fire Service of EMERCOM of Russia,
620062 Yekaterinburg, Russia

³ M.N. Mikheev Institute of Metal Physics, Ural Branch, Russian Academy of Sciences,
620108 Yekaterinburg, Russia

⁴ Institute of Solid State Chemistry, Russian Academy of Sciences, Ural Branch,
620990 Yekaterinburg, Russia

E-mail: larisamaskaeva@yandex.ru

Received July 31, 2021

Revised August 5, 2021

Accepted August 5, 2021

Polycrystalline films of $\text{Cd}_x\text{Pb}_{1-x}\text{S}$ ($0.021 \leq x \leq 0.090$) supersaturated substitutional solid solutions with a cubic structure $B1$ ($Fm\bar{3}m$ space group) have been obtained with varying cadmium acetate salt $\text{Cd}(\text{CH}_3\text{COO})_2$ in the reaction mixture within 0.01–0.10 mol/l on the sital substrates. Their thickness changed from ~ 0.4 to ~ 1.0 microns. A correlation has been established between the structural-morphological and functional properties of $\text{Cd}_x\text{Pb}_{1-x}\text{S}$ thin-film layers. The extreme character of the voltage sensitivity dependence on the cadmium salt concentration in the reaction bath is associated with the nonmonotonic introduction of cadmium into the PbS crystal lattice. It is shown that the maximum photocurrent is possessed by $\text{Cd}_x\text{Pb}_{1-x}\text{S}$ thin-film layers formed from crystallites with pronounced faceting. We have found the surface sensitivity of the $\text{Cd}_x\text{Pb}_{1-x}\text{S}$ films to the presence of $\sim 0.02 \text{ mg/m}^3$ NO_2 in the air, which is significantly lower than the maximum allowable concentration.

Keywords: chemical bath deposition, film morphology, structural properties, $\text{Cd}_x\text{Pb}_{1-x}\text{S}$ solid solution, photosensitivity, sensing properties.

DOI: 10.21883/SC.2022.14.53861.9726

1. Introduction

The interest in solid solutions based on $\text{A}^{\text{II}}\text{-B}^{\text{VI}}$ and $\text{A}^{\text{IV}}\text{-B}^{\text{VI}}$ semiconductor compounds, which expand the opportunities for modification of structural, semiconducting, and functional properties of single-metal chalcogenides and ensure their variable adjustment within a fairly wide range, has remained strong for a long time already. Thin-film lead sulfide PbS in its polycrystalline state is a narrow-bandgap semiconductor with a cubic ($Fm\bar{3}m$ space group) structure and a bandgap width of 0.41 eV at 300 K [1]. Owing to its photosensitivity in a wide spectral range of 0.4–3.0 μm , lead sulfide is applied in optoelectronic and sensor devices [2–5].

Cadmium sulfide with a wurtzite $B4$ ($P6_3mc$ space group) or sphalerite $B3$ structure ($F\bar{4}3m$ space group) is a wide-bandgap semiconductor with a bandgap width of 2.42 eV [6]. Cadmium sulfide is also used widely as a buffer layer in photovoltaic, optoelectronic, and photocatalytic devices.

Thin films of $\text{Cd}_x\text{Pb}_{1-x}\text{S}$ solid solutions with a variable bandgap width (0.4–2.42 eV), which cover the entire array of spectral properties of these compounds, are the most sought-after materials [7–13]. Adjusting the chemical composition, one may synthesize promising materials based on these compounds in a controlled way. Therefore, the fabrication of thin films of $\text{Cd}_x\text{Pb}_{1-x}\text{S}$ solid solutions with the use of cost-effective and simple methods for is a relevant

objective at present. The method of chemical deposition from aqueous media (chemical bath deposition, CBD) is the most attractive one in this context [4,8,11,13–19]. It is distinguished by the simplicity of process equipment and low-temperature process conditions. The method provides an opportunity to adjust the synthesis conditions (composition and concentrations of chemical reagents, process temperature and duration, nature of the substrate for deposition, etc.) and set such conditions that ensure the fabrication of $\text{Cd}_x\text{Pb}_{1-x}\text{S}$ films with the optimum properties for specific devices.

It follows from the analysis of scientific literature that the obtained data on properties and composition of thin-film $\text{Cd}_x\text{Pb}_{1-x}\text{S}$ solid solutions are contradictory, fragmentary, and are not always interpreted properly. This is attributable to the complexity and multifactorial nature of chemical deposition of films in question. These characteristics of the process preclude one from solving one of the fundamental problems of semiconductor materials science: determining the relation between structural and functional properties.

In view of the above, the aim of the present study was to perform a complex examination of the surface morphology, crystal structure, and sensing properties of thin films of $\text{Cd}_x\text{Pb}_{1-x}\text{S}$ solid solutions; to reveal the nature of changes occurring in them; and to determine the interrelations of parameters in the „synthesis–composition–structure–property“ series.

2. Experimental procedure

Thin-film layers in the CdS–PbS system, which were synthesized by chemical deposition from an ammonium-citric reaction bath containing 0.04 mol/L of lead acetate $\text{Pb}(\text{CH}_3\text{COO})_2$, 0.3 mol/L of sodium citrate $\text{Na}_3\text{C}_6\text{H}_5\text{O}_7$, 4.5 mol/L of ammonium hydroxide NH_4OH , and 0.58 mol/L of thiourea $\text{N}_2\text{H}_4\text{CS}$ (source of sulfide ions), were studied. The concentration of cadmium acetate $\text{Cd}(\text{CH}_3\text{COO})_2$ was varied within the range from 0.01 to 0.10 mol/L. The deposition of films was performed within 120 min at a temperature of 353 K in sealed reactors made of molybdenum glass. Degreased sital ST-50-1 substrates secured in fluoropolymer holding fixtures were introduced into them. The reactors were mounted in a „TS-TB-10“ thermostat with an accuracy of temperature control of ± 0.1 K. Following synthesis, the films were rinsed with distilled water and dried in air.

The thickness of the produced films was determined using an MII-4M interference microscope (Linnik microinterferometer) with a measurement error of 20%.

The microstructure and the elemental composition of films of $\text{Cd}_x\text{Pb}_{1-x}\text{S}$ solid solutions were examined by high-resolution scanning electron microscopy using a MIRA 3 LMU microscope at an accelerating electron-beam voltage of 10 kV and a JEOL JSM-5900 LV microscope with an EDS Inca Energy 250 energy-dispersive X-ray analyzer.

X-ray diffraction studies were conducted using two diffractometers: a laboratory PANalytical Empyrean Series 2 instrument (CuK_α radiation, parallel beam geometry) with a position-sensitive PIXel3D detector providing a 2θ resolution no worse than 0.0016 and a standard industrial Dron-4 diffractometer. Measurements were carried out in the standard Bragg–Brentano diffraction geometry in a 2θ interval from 20 to 80°. The composition and the structural parameters of $\text{Cd}_x\text{Pb}_{1-x}\text{S}$ films were determined by full-profile Rietveld analysis [20,21] with the use of the Fullprof software [22]. The conventional Williamson–Hall plot was used to determine the size of particles forming $\text{Cd}_x\text{Pb}_{1-x}\text{S}$ films and the emerging strain [23]:

$$\beta \cdot \cos \theta = 0.9\lambda/D + 4\varepsilon \cdot \sin \theta,$$

where D is the average size of coherent scattering regions, which is assumed to be the average size of particles; β is the reflection FWHM in radians; λ is the wavelength of X-ray radiation; $\varepsilon = \Delta d/d$ is the strain; and d is the interplanar distance.

The conductivity type of films was determined by checking the sign of thermal emf in experiments where a temperature gradient was created in the region of probe contacts.

The photovoltaic characteristics (dark resistance R_d and voltage sensitivity U_s) of CdPbS films were measured using a K.54.410 setup with a black body 573 K radiation source at a modulation frequency of 800 Hz and an irradiance of $1 \cdot 10^{-4}$ W/cm².

The current–voltage curves (CVCs) of the synthesized films were recorded at 298 K and an applied voltage varying from -10 to 10 V with a pitch of 100 mV by the two-probe method both in darkness and under illumination (100 mW/cm^2) by a light beam from a Zolix GLORIA-X500A solar simulator fitted with an Osram XBO 500W/H OFR lamp. The current strength was determined using a Keithley 2450 sourcemeter.

Sensor elements with a sensing area 5×5 mm were fabricated based on films of $\text{Cd}_x\text{Pb}_{1-x}\text{S}$ solid solutions. These elements had electrochemically deposited nickel electric contacts. The Ohmic resistance of films was measured with a Shch 301-1 combined instrument. The sensing properties of films with regard to nitrogen dioxide were examined in a specially designed sealed cell. A sensor element was secured with pressure contacts inside it, and a gas–air mixture was then introduced. Gaseous mixtures used in these experiments had an initial concentration of nitrogen dioxide in air of 0.08, 8.0, 40, and 200 mg/m³. The temperature of these mixtures was 295 K, and the pressure was atmospheric.

3. Results and discussion

3.1. Morphology studies

The dependence of the thickness of synthesized layers in the PbS–CdS system on the concentration of cadmium acetate in the reaction mixture (with the concentrations of other system components being fixed) is extremal in nature. As the concentration of $\text{Cd}(\text{CH}_3\text{COO})_2$ grows from 0.01 to 0.08 mol/L, the semiconducting layer thickness increases monotonically from ~ 0.5 to $\sim 1.0 \mu\text{m}$. At a cadmium acetate concentration of 0.1 mol/L in the reactor, the $\text{Cd}_x\text{Pb}_{1-x}\text{S}$ layer thickness decreases abruptly to $\sim 0.6 \mu\text{m}$. The kinetic data suggest that this is the result of redistribution of lead and cadmium sulfides to the precipitate.

The size and shape of grains define structural and functional properties and are the key parameters of the thin-film ternary CdPbS compound on dielectric substrates. Electron microscope images of $\text{Cd}_x\text{Pb}_{1-x}\text{S}$ films with the cadmium acetate concentration varying from 0.01 to 0.10 mol/L in the reaction mixture and the size spread of grains, which is presented in the form of an FWHM value of the approximating Gaussian curve, are shown in Fig. 1. Well-faceted crystallites in the shape of octahedra, tetrahedra, or truncated polyhedra of the cubooctahedron type with various sizes and orientations relative to the substrate plane form on sital substrates throughout the entire range of concentrations of cadmium salt in the solution. The exception is a film obtained at a concentration of 0.04 mol/L of $\text{Cd}(\text{CH}_3\text{COO})_2$ in the reactor. It has a radically different microstructure: crystallites in it turn into planar grains with rounded facets and irregular edges. Since the shape of grains is not regular and the images are two-dimensional, the so-called statistical diameter (Martin

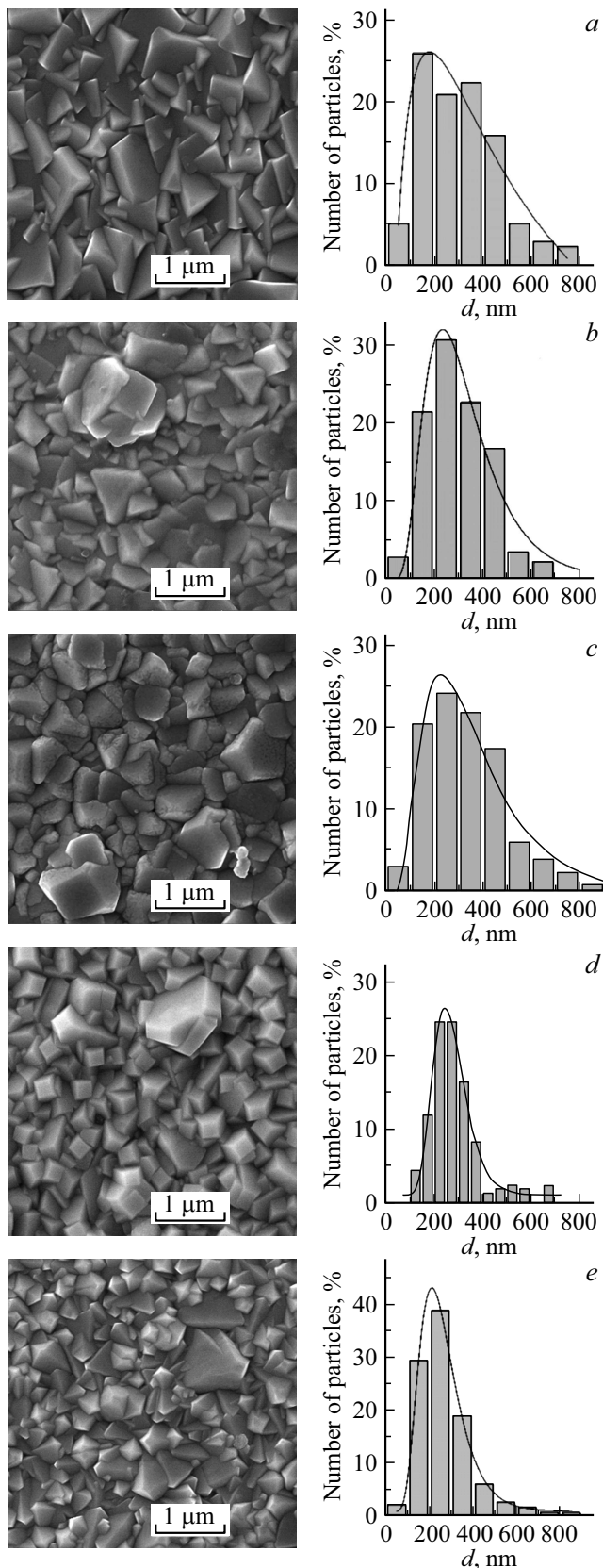


Figure 1. Electron microscope images of CdPbS films deposited onto sitall substrates from the reaction mixture containing $Cd(CH_3COO)_2$, mol/L: 0.01 (a), 0.02 (b), 0.04 (c), 0.08 (d), 0.10 (e). The FWHM values of approximating Gaussian curves characterizing the size spread of grains are presented on the right.

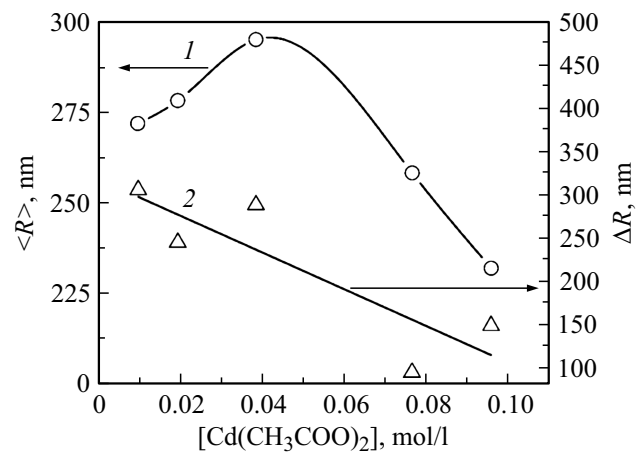


Figure 2. Dependences of (1) the average size of grains forming a CdPbS film on sitall in the process of chemical deposition from a reaction bath with various concentrations of $Cd(CH_3COO)_2$ and (2) the FWHM of approximating Gaussian curves characterizing the size spread of grains.

diameter) was estimated. This diameter was taken to be the length of a bisector that divides the grain projection area into two approximately equal parts.

The Gaussian distribution of the average grain size ($\langle R \rangle$) and the size spread of grains determined based on the FWHM of the approximating Gaussian curve (ΔR) plotted against the cadmium acetate concentration in the reactor (Fig. 2) were used to analyze the CdPbS film morphology. As the cadmium salt concentration grows from 0.01 to 0.04 mol/L, the average size of grains forming the CdPbS film increases from 270 to ~300 nm. When the cadmium salt concentration increases further, the size drops to 260 and 230 nm at 0.08 and 0.1 mol/L, respectively.

The grain size variation determined based on the FWHM of the approximating Gaussian curve (ΔR) behaves differently. In this estimation, the size of grains decreases monotonically (and their homogeneity improves) as the $Cd(CH_3COO)_2$ concentration in the reaction bath grows (Fig. 2). Thus, the identified morphological features of crystallites in films on sitall are preserved within the entire studied range of the cadmium salt concentration in the reactor, but their size and mean deviation from it vary.

It follows from the analysis of the obtained results that the identified morphological features of films are likely to be governed by the concentration of cadmium acetate in the reaction bath and the conditions of nucleation and growth of layers on the substrate. The substrates used in the study are made of ST-50-1 sitall, which is a glass-ceramic semi-crystalline material containing „catalytic additives“. These substrates facilitate the emergence of a large number of nucleation sites and establish the conditions needed to form a polycrystalline structure. Thus, the results of electron microscope investigations demonstrated that the cadmium salt concentration exerts a consider-

able influence on the microstructure of deposited CdPbS films.

3.2. Crystal structure

The structural state (i.e., crystal lattice type, grain size, defect density, and internal microstresses) is another key parameter that governs, together with morphology, the photovoltaic and sensing properties of synthesized films in the CdS–PbS system. In most studies, the sizes of crystallites are determined based on the broadening of individual X-ray scattering lines, and the probable contribution from other structural parameters is neglected. In the present study, we performed a comprehensive examination of the structural state of CdPbS films using the entire range of scattering angles (X-ray diffraction profile). This helped obtain more accurate and reliable results. Simulations in the FullProf software, where full-profile Rietveld analysis is implemented, were conducted for this purpose.

A set of diffraction reflections typical of a cubic face-centered lattice of the NaCl type ($B1$, $Fm\bar{3}m$ space group) is present in the diffraction patterns of CdPbS films shown in Fig. 3. All of them feature well-pronounced near-Gaussian or near-Lorentzian curve shapes and relatively narrow reflections; i.e., it is fair to state that almost all of the studied ternary layers are polycrystalline.

The shift of all diffraction reflections toward larger 2θ values (Fig. 3), the fragment of diffraction patterns with reflection $(311)_{B1}$, which is equivalent to a reduction in period a_{B1} , is a convincing proof of the formation of substitution solid solutions $Cd_xPb_{1-x}S$. The observed a_{B1} reduction from 0.59242(1) to 0.58918(1) nm (Table 1) is attributable to the substitution of lead ions Pb^{2+} (0.120 nm) with cadmium ions Cd^{2+} (0.097 nm) in the PbS lattice. The results of quantitative analysis of the diffraction patterns also allowed us to estimate the value of x in $Cd_xPb_{1-x}S$ solid solutions (i.e., the relative concentration of cadmium in the metal sublattice). The relative concentration of Cd in a substitution solid solution was estimated in accordance with the Vegard law as $x = (a_{PbS} - a_{ss}) / (a_{PbS} - a_{CdS})$, where a_{PbS} , a_{CdS} , and a_{ss} are the lattice parameters of lead sulfide, cadmium sulfide, and the $Cd_xPb_{1-x}S$ substitution solid solution. The lattice parameter of a PbS film ($a_{PbS} = 0.59332$ nm) synthesized from the reaction bath with no cadmium salt was used to calculate x . Since the cubic PbS structure is preserved in substitution solid solutions $Cd_xPb_{1-x}S$, it may be assumed that the cadmium sulfide lattice distorts into a cubic one in the region of limited solubility. Therefore, the period of a model cubic CdS lattice cell, which was determined theoretically using an empirical size of Cd^{2+} cations in the six-fold environment in the NaCl lattice, is $a_{CdS} = 0.546$ nm. The calculated concentration of cadmium in the PbS lattice (see Table 1) is indicative of the formation of highly supersaturated substitution solid solutions $Cd_xPb_{1-x}S$ ($0 \leq x \leq 0.09$). Since the synthesis of films was performed at 353 K, the achieved level of

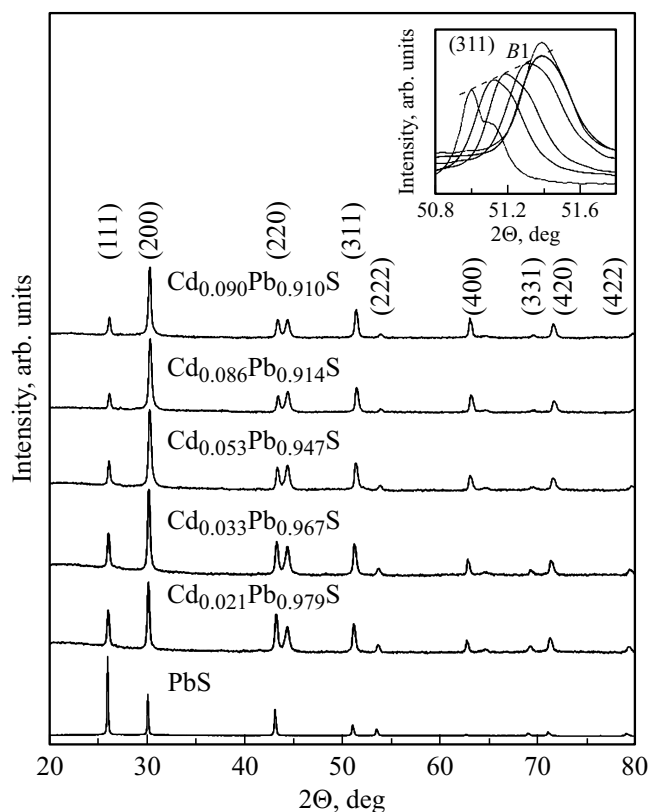


Figure 3. Experimental X-ray diffraction patterns of films of $Cd_{0.021}Pb_{0.979}S$, $Cd_{0.033}Pb_{0.967}S$, $Cd_{0.053}Pb_{0.947}S$, $Cd_{0.086}Pb_{0.914}S$, and $Cd_{0.090}Pb_{0.910}S$ solid solutions synthesized by chemical deposition onto a siall substrate from the reaction bath containing $Cd(CH_3COO)_2$, mol/L: 0.01, 0.02, 0.04, 0.08, 0.1. The inset illustrates the shift of reflection $(311)_{B1}$ of solid solutions $Cd_xPb_{1-x}S$ toward larger 2θ angles in the case of substitution of Pb atoms with Cd atoms.

supersaturation in CdS is more than 4 orders of magnitude higher than the equilibrium phase diagram values for the PbS–CdS system [24].

The gradual variation of the intensity ratio of reflections $(111)_{B1}$ and $(200)_{B1}$ with concentration of $Cd(CH_3COO)_2$ in the reactor (Fig. 3) is another feature of the obtained X-ray diffraction patterns that is indicative of the formation of substitution solid solutions in the CdS–PbS system. The ratio of intensities of reflections $(111)_{B1}$ and $(200)_{B1}$ demonstrates that partial alignment of grains with the preferred crystallographic plane (200) was established in films.

The dimensional and strain contributions to the broadening of reflections were separated to estimate the average grain size and microstrain. This evaluation done in a traditional manner using the example of an X-ray diffraction pattern for a $Cd_{0.021}Pb_{0.979}S$ solid solution film synthesized from the reaction bath with 0.01 mol/L of $Cd(CH_3COO)_2$ (Fig. 4). The inset shows the angular dependence of physical broadening in the form of a dependence of $\beta \cdot (2\theta) \cdot \cos \theta$ on $\sin \theta$. The slope of these dependences is indicative of particle strain, while the y-intercept ($\sin \theta = 0$) yields the

Table 1. Crystal lattice parameter a_{B1} , cadmium concentration x in films of $Cd_xPb_{1-x}S$ solid solutions, number of grains with the preferred (200) orientation parallel to the substrate plane $T_{(200)}$, size of coherent scattering regions (CSRs) D , and average microstrain value $\Delta d/d$

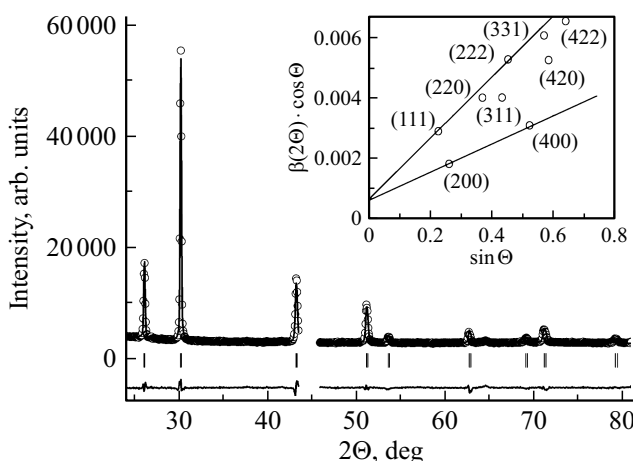
$Cd(CH_3COO)_2$, mol/l	0.01	0.02	0.04	0.08	0.10
a_{B1} , nm	0.59242(1)	0.59187(1)	0.59094(1)	0.58951(1)	0.58918(1)
x in $Cd_xPb_{1-x}S$	0.021	0.033	0.053	0.086	0.090
$T(200)$, %	6	26.2	32.3	34.9	24.2
D , nm	227	232	302	300	324
$\Delta d/d \cdot 10^4$	8.84	9.38	14.9	18.3	18.9

size of particles. A similar procedure was applied to all diffraction spectra.

Average sizes of grains forming films of $Cd_xPb_{1-x}S$ solid solutions and volume-average microstrain values for various concentrations of cadmium acetate in the reaction bath are listed in Table 1.

Size D of coherent scattering regions, which is a first approximation to the average grain size, increases from 227 to 324 nm (and the value of microstrain in the bulk of a film increases by a factor of ~ 2) as the cadmium salt concentration grows from 0.01 to 0.1 mol/L.

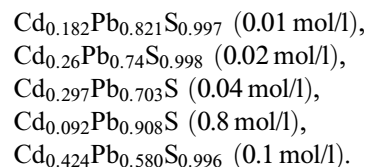
Local energy-dispersive elemental microanalysis (EDX) was performed at no less than 10 points spread over the entire layer surface area in order to determine the elemental composition of the synthesized films. The averaged results of elemental analysis for lead, cadmium, and sulfur listed in Table 2 suggest that the cadmium salt concentration in the reaction mixture exerts a considerable influence on the film composition. As the $Cd(CH_3COO)_2$ salt concentration in the reactor varies from 0.01 to 0.04 mol/L, the concentration of cadmium in the CdPbS film composition increases from

**Figure 4.** Experimental (points) and calculated (envelope line) X-ray diffraction patterns for the $Cd_xPb_{1-x}S$ solid solution film deposited from the reaction bath containing 0.01 mol/L of $Cd(CH_3COO)_2$. The lower line is the difference between the calculated and experimental X-ray diffraction patterns. Line marks denote the angular positions of peaks of the $B1$ phase. The inset shows the dependence of $\beta \cdot (2\theta) \cdot \cos \theta$ on $\sin \theta$.**Table 2.** Results of energy-dispersive elemental microanalysis of thin-film CdPbS compounds for various concentration of cadmium acetate in the reaction mixture

Element, at%	0.01	0.02	0.04	0.08	0.10
Cd	9.10	13.04	14.83	4.60	21.20
Pb	41.06	37.06	35.17	44.65	28.98
S	49.83	49.90	50.01	50.75	49.82

9.1 to 14.83 at%. When the cadmium salt concentration in the reactor increases further to 0.08 mol/L, the fraction of Cd in the film drops to 4.60 at%; at 0.1 mol/L, it increases sharply to 21.20 at%.

The overall concentration of metals (Cd + Pb) in films remains higher than the one of sulfur (chalcogen) up to cadmium salt concentrations of 0.01 and 0.02 mol/L in the reactor, in which case the layer is formed by well-faceted crystallites covering the substrate surface (Fig. 1, a, b). The composition of the film formed at 0.04 mol/L of $Cd(CH_3COO)_2$ in the reaction bath corresponds to the stoichiometric relation between the sum of metals and the chalcogen; at 0.08 mol/L, excess sulfur is present in the layer (50.75 at%). At the maximum concentration of cadmium salt in the reactor, an excess of metals is seen again in the synthesized layer. According by the EDX data, the formular composition of layers synthesized in this study at different concentrations of cadmium salt in the reaction bath should be written in the following way:



Therefore, all films (except for the film layer obtained with 0.08 mol/L of cadmium acetate in the reaction mixture) contain an amorphous CdS phase in addition to the solid solution.

Thus, polycrystalline films of supersaturated substitution solid solutions $Cd_xPb_{1-x}S$ with cubic structure $B1$ ($Fm\bar{3}m$ space group) were synthesized by chemical deposition with the cadmium acetate concentration in the reaction bath varying from 0.01 to 0.1 mol/L. The discussed thin-film

compounds contain a solid solution alone or a solid solution together with an amorphous cadmium sulfide phase.

According to the results of electron microscope investigations and X-ray diffraction studies, the surface morphology and the structural state of the discussed films vary nonmonotonically with $\text{Cd}(\text{CH}_3\text{COO})_2$ concentration in the reactor, thus potentially providing a wide variety of functional properties.

3.3. Photosensitivity and sensing properties

The synthesized $\text{Cd}_x\text{Pb}_{1-x}\text{S}$ compounds have an advantage in that their functional properties vary widely with composition, morphology, crystal structure, degree of supersaturation of the solution with respect to cadmium, and conductivity type. This allows one to „tune“ semiconducting layers to exhibit photoelectric emission under illumination or selective chemical reactivity with toxic gases.

It can be seen from Fig. 5 that compositional and morphological variations affected the photovoltaic properties of the studied films (specifically, voltage sensitivity U_s (1) under infrared illumination and dark resistance R_d (2)). The voltage photosensitivity of films of $\text{Cd}_x\text{Pb}_{1-x}\text{S}$ solid solutions deposited from reaction baths increases by a factor of ~ 2 as the concentration of $\text{Cd}(\text{CH}_3\text{COO})_2$ grows from 0.01 to 0.04 mol/L. When the cadmium acetate concentration increases further to 0.08 mol/L in the reactor, the voltage sensitivity of the studied layers drops sharply and assumes near-zero values in a film synthesized at the maximum cadmium salt concentration (0.1 mol/L).

As for dark resistance R_d , its dependence on the cadmium acetate concentration in the reaction bath is more complex in nature: its first increases monotonically from ~ 70 to $\sim 350 \text{ M}\Omega/\text{sq}$ and then decreases to $\sim 70 \text{ M}\Omega$. The subsequent jump of R_d to $1000 \text{ M}\Omega/\text{sq}$ in a film with the $\text{Cd}_{0.424}\text{Pb}_{0.580}\text{S}_{0.996}$ formula composition is related to the fact that this film contains, in addition to the $\text{Cd}_{0.09}\text{Pb}_{0.91}\text{S}$ solid solution, a considerable amount of amorphous cadmium sulfide.

The comparison of measured photovoltaic characteristics U_s and R_d with the results of X-ray diffraction and EDX studies suggests that a certain critical amount of the amorphous CdS phase in a semiconducting layer facilitates the enhancement of its photosensitivity. Specifically, the film with the $\text{Cd}_{0.297}\text{Pb}_{0.703}\text{S}$ (0.04 mol/L) formula composition, which has the highest voltage sensitivity, contains the $\text{Cd}_{0.053}\text{Pb}_{0.947}\text{S}$ solid solution and amorphous CdS in the amount that is (presumably) optimum in the given conditions. The film containing the $\text{Cd}_{0.086}\text{Pb}_{0.914}\text{S}$ solid solution only, which was synthesized at 0.08 mol/L of cadmium acetate in the reaction bath, has moderate signal U_s values.

The CVCs (a) and the current density (b) of the discussed $\text{Cd}_x\text{Pb}_{1-x}\text{S}$ layers measured under illumination with a light beam from a solar simulator and at different concentrations of cadmium acetate in the reaction bath are shown in Fig. 6. The CVCs are symmetric and linear at applied voltages

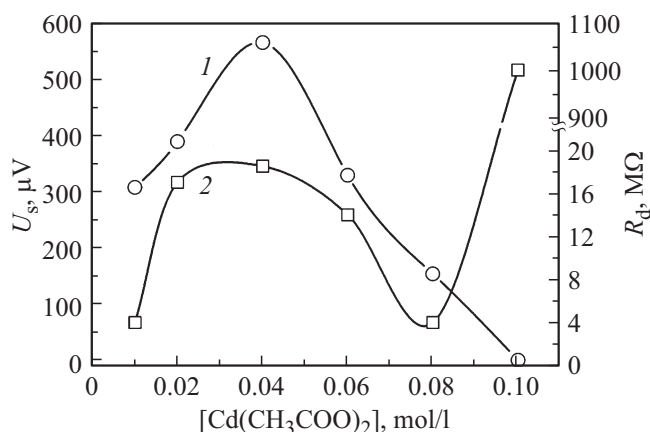


Figure 5. Dependences of voltage sensitivity U_s (1) and dark resistance R_d (2) of films of $\text{Cd}_x\text{Pb}_{1-x}\text{S}$ solid solutions on the $\text{Cd}(\text{CH}_3\text{COO})_2$ concentration in the reaction bath.

ranging from -10 to 10 V . The light and dark current densities as functions of the cadmium salt concentration in the reaction bath have asymmetric dependences of voltage sensitivity $U_s = f[\text{Cd}(\text{CH}_3\text{COO})_2]$ with a minimum at point corresponding to 0.04 mol/L of $\text{Cd}(\text{CH}_3\text{COO})_2$, where the disruption of crystallites and the formation of grains with irregular edges are observed. As was already noted in [25], thin-film compounds with clear-cut crystallographic faceting of crystallites feature the highest photocurrent values. In the present study, these are the layers synthesized at 0.01 and 0.08 mol/L of cadmium acetate in the reactor.

The discussed thin films based on lead and cadmium sulfides may also be used to construct thin-film chemical sensors (specifically, to detect certain toxic gases in air environment).

We have demonstrated in [26] that thin films of $\text{Cd}_x\text{Pb}_{1-x}\text{S}$ solid solutions have a fairly low detection threshold for nitrogen dioxide NO_2 in air. This is especially apparent when cadmium acetate is introduced into the reaction bath in the process of chemical deposition of solid solutions [8]. However, the influence of the cadmium acetate concentration on the surface sensitivity properties of sensor elements based on $\text{Cd}_x\text{Pb}_{1-x}\text{S}$ has not been examined yet. The operating principle of chemical sensors is that their electrophysical characteristics change when they absorb nitrogen dioxide. Specifically, following contact with gas, Ohmic resistance R_r of a film changes (decreases or increases) relative to its initial value R_0 . In the present study, we fabricated sensor elements $5 \times 5 \text{ mm}$ in size from $\text{Cd}_x\text{Pb}_{1-x}\text{S}$ layers synthesized with various concentrations of cadmium acetate in the reaction mixture. The gas sensitivity of sensors was estimated by the variation of ratio R_0/R_r on contact with gas. As it turned out, the conductivity type of synthesized films, which was determined in advance, exerts a decisive influence on the nature of variation of the Ohmic resistance. Specifically, layers of binary PbS and $\text{Cd}_x\text{Pb}_{1-x}\text{S}$ solid solutions with a

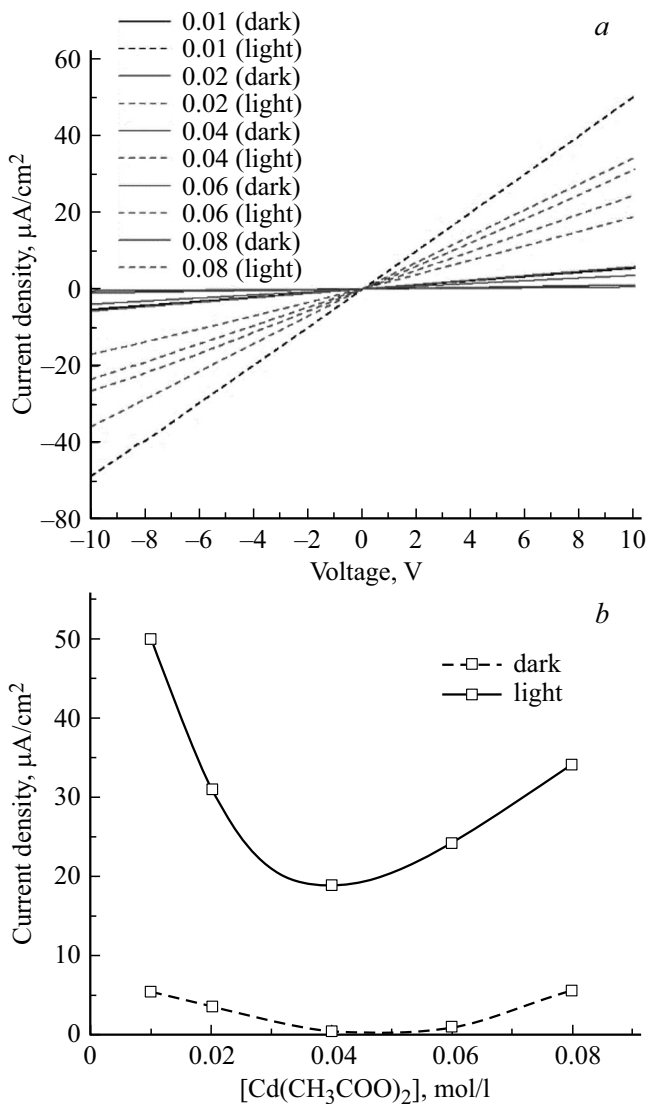


Figure 6. Current–voltage curves (a) and dependence of the current density (b) on the concentration of cadmium acetate in the reaction bath.

relatively low cadmium concentration ($0 \leq x \leq 0.033$) are *n*-type semiconductors, while films of solid solutions with higher cadmium concentrations ($0.053 \leq x \leq 0.09$) are *p*-type semiconductors. These types of films exhibited opposite Ohmic resistance variations on contact with NO_2 : R_τ decreased in the former case and increased in the latter case.

The concentration and kinetic dependences of the response of sensor elements shown in Fig. 7 reveal a correlation between the concentration of detected gas in the gas phase and the variation (increase or decrease) of Ohmic resistance of thin-film elements. The sensor element based on undoped lead sulfide (1), which is the base compound for $Cd_xPb_{1-x}S$ solid solutions, does not reveal any appreciable gas-sensing properties up to a nitrogen dioxide concentration of 20 mg/m^3 . The R_0/R_τ ratio then increases sharply by a factor of ~ 1.5

at 200 mg/m^3 (Fig. 7, a). When the thin-film sensor element based on a $Cd_{0.021}Pb_{0.979}S$ (2) solid solution comes into contact with NO_2 , the relative resistance variation starts increasing already at a gas concentration of 0.1 mg/m^3 in air environment and exceeds the initial R_0/R_τ value by a factor of ~ 2.4 . The R_0/R_τ ratio of the $Cd_{0.033}Pb_{0.967}S$ (3) film in contact with nitrogen dioxide increases in a similar fashion (although at a lower rate), while the $Cd_{0.086}Pb_{0.914}S$ (4) film does not exhibit any useful gas-sensing properties. If

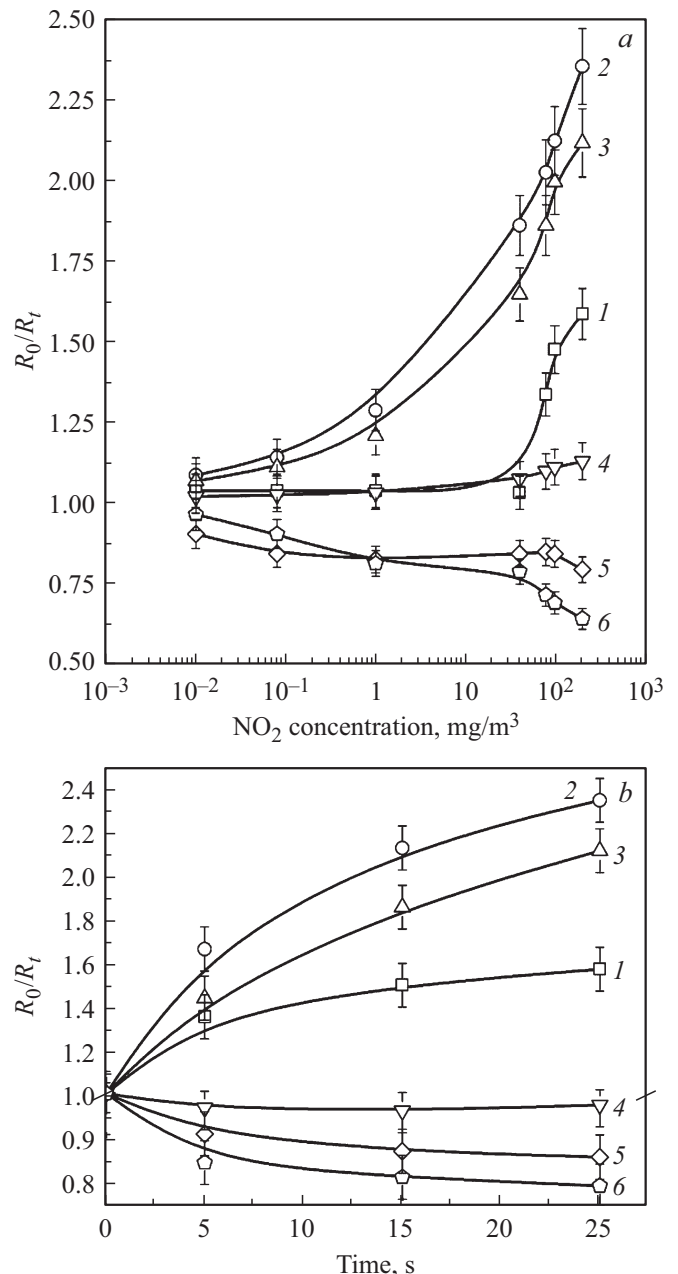


Figure 7. Concentration (a) and kinetic (b) dependences of variation of Ohmic resistance ratio R_0/R_τ of films synthesized from the reaction mixture containing $Cd(CH_3COO)_2$, mol/L: 0 (1), 0.01 (2), 0.02 (3), 0.04 (4), 0.08 (5), 0.1 (6). The duration of contact of sensor elements with nitrogen dioxide was 25 s (a), and the NO_2 concentration was 200 mg/m^3 (b).

one uses sensor elements based on $\text{Cd}_{0.086}\text{Pb}_{0.914}\text{S}$ (5) and $\text{Cd}_{0.09}\text{Pb}_{0.91}\text{S}$ (6) solid solutions, R_0/R_τ decreases by 20 and 40%, respectively.

The kinetic dependences in Fig. 7, *b* reveal a fairly high rate of adsorption interaction of sensor elements with gas: the R_0/R_τ relative resistance variation reaches 15–60% (depending on concentration x in $\text{Cd}_x\text{Pb}_{1-x}\text{S}$) within the first 5 s of contact with NO_2 . Notably, a prolonged contact of a film with gas does not alter the nature of dependences and just yields higher absolute values of the sensor response, which reaches saturation by the 15th second of contact for films synthesized in the presence of 0.04 (4), 0.08 (5), and 0.1 (6) mol/L of $\text{Cd}(\text{CH}_3\text{COO})_2$ in the reaction bath. Sensor elements fabricated based on films synthesized with the minimum concentrations of cadmium salt (0.01 and 0.02 mol/L) in the reactor provide a 110–130% growth of R_0/R_τ relative to the initial state in a 25-s-long contact with NO_2 .

When sensor elements were removed from the measurement cell with NO_2 into clean air, their Ohmic resistance returned to its initial value R_0 at room temperature within a time ranging from several minutes to 2–3 h. This is indicative of the physical nature of interaction of thin-film $\text{Cd}_x\text{Pb}_{1-x}\text{S}$ layers with nitrogen dioxide.

4. Conclusion

Polycrystalline CdPbS films with their thickness varying from 0.5 to $\sim 1.0\ \mu\text{m}$ were synthesized by chemical deposition from an ammoniac-citric reaction bath. The nonlinear evolution of microstructure of thin-film layers on siall substrates with concentration of cadmium acetate in the reaction bath, which varied from 0.01 to 0.1 mol/L, was revealed in electron microscopical investigations.

The formation of supersaturated $\text{Cd}_x\text{Pb}_{1-x}\text{S}$ ($x \leq 0.09$) solid solutions with a cubic face-centered lattice of the NaCl type (*B1*, space group $Fm\bar{3}m$) at cadmium concentrations of 0.01–0.1 mol/L in the reactor was verified by X-ray diffraction. Full-profile analysis of X-ray diffraction patterns with computer simulations in the FullProf software and the „modified“ Williamson–Hall plot were used to perform a complex examination of the size of crystallites forming a film, the degree of their texturing, and the microstrain values for films of $\text{Cd}_x\text{Pb}_{1-x}\text{S}$ solid solutions deposited onto siall substrates.

The nature of variation of voltage sensitivity, photocurrent, and sensor response to NO_2 in air of films of $\text{Cd}_x\text{Pb}_{1-x}\text{S}$ solid solutions with their structural and morphological parameters and synthesis conditions was determined.

Funding

This study was supported financially by the Ministry of Science and Higher Education of the Russian Federation (project No. FEUZ-2020-0058 (N687.42B.223/20), grant 20-48-660041r_a from the Russian Foundation for

Basic Research, and as part of the state assignment of the Ministry of Education and Science of the Russian Federation (project „Flux“ No. AAAA-A18-118020190112-8).

Conflict of interest

The authors declare that they have no conflict of interest.

References

- [1] W.W. Scanlon. *J. Phys. Chem. Solids*, **8**, 423 (1959).
- [2] P.M. Khanzode, D.I. Halge, V.N. Narwade, J.W. Dadge, K.A. Bogle. *Optik*, **226** (1), 165933 (2020).
- [3] E. Pentia, V. Draghici, G. Sarau. *J. Electrochem. Soc.*, **151** (11), G729 (2004).
- [4] A. Ounissi, N. Ouddai, S. Achour. *Eur. Phys. J. Appl. Phys.*, **37** (3), 241 (2007).
- [5] V. Rakovics. *Mat. Res. Soc. Symp. Proc.*, **900**, 87 (2005).
- [6] A.E. Rakhshani, B. Pradeep, H.A. Ramazaniyan. *Chem. Sol. Deposit. of Semicond. and Non-Metal. Films: Proc. Int. Symp. Electrochem. Soc.*, **32**, 49 (2006).
- [7] P.L. Nichols, Z. Liu, L. Yin, S. Turkdogan, F. Fan, C.Z. Ning. *Nano Lett.*, **15**, 909 (2015).
- [8] A.E. Bezdetnova, V.F. Markov, L.N. Maskaeva, Yu.G. Shashmurin, A.S. Frants, T.V. Vinogradova. *J. Anal. Chem.*, **74** (12), 1256 (2019).
- [9] D.A. Caselli, C.Z. Ning. *Opt. Express*, **19** (S4), A686 (2011).
- [10] G.L. Tan, L. Liu, W. Wu. *AIP Adv.*, **4**, 067107 (2014).
- [11] K.E. Suryavanshi, R.B. Dhake, A.M. Patil, M.R. Sonawane. *Optik*, **218**, 165008 (2020).
- [12] R.K. Dutta. *Nat. Sci.*, **9** (1), 21 (2020).
- [13] L.N. Maskaeva, E.V. Mostovshchikova, I.V. Vaganova, V.F. Markov, V.I. Voronin, A.D. Kutyavina, E.G. Vovkotrub. *Thin Sol. Films*, **718**, 138468 (2020).
- [14] V.F. Markov, L.N. Maskaeva, P.N. Ivanov. *Gidrokhimicheskoe osazhdenie plenok sulfidov metallov: modelirovanie, eksperiment* (Ekaterinburg, Ural. Otd. Ross. Akad. Nauk, 2006) (in Russian).
- [15] S. Rajathi, K. Kirubavathi, K. Selvaraju. *J. Taibah Univ. for Sci.*, **11** (6), 1296 (2017).
- [16] S.R. Deo, A.K. Singh, L. Deshmukh, L.J. Paliwal, R.S. Singh. *Optik*, **126** (20), 2311 (2015).
- [17] M.A. Barote, S.S. Kamble, L.P. Deshmukh, E.U. Masumdar. *Ceram. Int.*, **39** (2), 1463 (2013).
- [18] S.M. Ho. *Int. J. Thin. Films Sci. Technol.*, **10** (1), 45 (2021).
- [19] A. Mohammed, Ali M. Mousa, J.P. Ponpon. *J. Semicond. Technol. Sci.*, **9** (2), 117 (2009).
- [20] H.M. Rietveld. *J. Appl. Crystallogr.*, **2** (2), 65 (1969).
- [21] D.L. Bush, J.E. Post. *Rev. in Min.*, **20**, 369 (1990).
- [22] J. Rodrigues-Carvajal. *Physica B*, **192** (1–2), 55 (1993).
- [23] G.K. Williamson, W.H. Hall. *Acta Metall.*, **1** (1), 22 (1953).
- [24] L.E. Shelimova, V.N. Tomashik, V.I. Grytsiv. *Diagrammy sostoyaniya v poluprovodnikovom materialovedenii (sistemy na osnove khal'kogenidov Si, Ge, Sn, Pb)* (M., Nauka, 1991), Chap. 9, p. 256 (in Russian).
- [25] L.N. Maskaeva, E.V. Mostovshchikova, V.F. Markov, V.I. Voronin, A.V. Pozdin, I.O. Selyanin, A.I. Mikhailova. *Semiconductors*, **56** (2), 91 (2022).
- [26] V.F. Markov, L.H. Maskaeva, Yu.S. Polikarpova, M.P. Mironov, V.N. Rodin, L.S. Solov'ev, B.V. Berg, V.N. Potapov. RF Patent 2305830 (in Russian). Application 2006115277/28 dated May 3, 2006, publ. September 10, 2007.